Decoding RSSI Compression in RFID: Dynamic RCS Modeling and Tag-Intrinsic Power Metrics for Reliable Backscatter Networks

Jia Liu[†*] Yifei Ma[†] Xingyu Chen[†] Haipeng Dai[†] He Huang[‡] Zihao Lin[†] Wei Zheng[†]
Junzhao Du[§] Guihai Chen[†]
[†] *State Key Laboratory for Novel Software Technology, Nanjing University*
[‡] *School of Computer Science and Technology, Soochow University*
[§] *School of Computer Science and Technology, Xidian University*

Abstract

Radio Frequency Identification (RFID) is a foundational element of modern IoT and backscatter networks, powering inventory, localization, and battery-free sensing at scale. In this paper, we uncover *RSSI compression*, a power-dependent bias in reader-measured RSSI, as a critical physical-layer problem that propagates upward in the network stack, degrading MAC-layer collision resolution, network-layer link estimation, and application-layer reliability. Through carefully designed experiments, we trace this distortion to dynamic tag Radar Cross Section (RCS) behavior and introduce two novel physical-layer metrics: *Interrogation Threshold Power* (ITP), a channel-specific metric for accurate link-quality estimation, and *Backscatter Power Index* (BPI), a tag-intrinsic, environment-agnostic signature. These metrics provide high-fidelity signal information that higher layers can directly exploit for more robust collision detection, power control, localization and sensing tasks. Finally, an in-situ single-query method further reduces measurement overhead by 99.8%, while cutting channel-estimation error by 64.7%, delivering significant cross-layer performance gains in real-world backscatter networks.

1 Introduction

Radio Frequency Identification (RFID) systems are a cornerstone of modern IoT and backscatter networks, enabling large-scale inventory management [9, 11, 40, 45], asset tracking [24, 30, 37, 41, 44], and battery-free sensing [15, 23, 36, 43] across industries such as logistics, retail, and smart manufacturing. As these deployments scale to tens of thousands of tags and multiple readers, maintaining reliable connectivity and efficient communication across the network stack becomes increasingly challenging. In such environments, physical-layer anomalies often propagate upward, degrading MAC-layer collision resolution [27], network-layer link estimation [28], and application-layer reliability [19].

One newly observed anomaly is *RSSI compression* – a power-dependent bias in reader-measured Received Signal Strength Indicator (RSSI) caused by the nonlinear Radar Cross Section (RCS) response of passive tags. Conventional RFID protocols rely on RSSI as a lightweight indicator of link quality, feeding it into MAC-layer collision detection, network-layer link estimation, and application-level sensing and localization. When RSSI measurements become distorted, these layers suffer: Collision resolution may misallocate slots, power-control policies may select suboptimal settings, link-quality estimation for multi-reader handovers may become unreliable, and application services such as real-time inventory or localization may experience reduced accuracy and higher latency. For example, in a warehouse with thousands of tags, compressed RSSI values cause the system to overestimate link quality (leading to missed tag reads) or underestimate it (triggering unnecessary retransmissions that increase network contention), inflating latency and network contention. We detail how our study mitigates these cross-layer issues in Section 5.2. Although a few prior studies have noted RSSI inconsistencies [26], the root causes, quantitative characterization, and cross-layer consequences of RSSI compression remain poorly understood, leaving a critical gap in the design of robust and efficient RFID backscatter networks.

To address this challenge, we first conduct carefully designed experiments to trace RSSI compression to its physical-layer root cause: The dynamic, power-dependent behavior of tag RCS, which exhibits up to 30 dB variations across operational ranges. Building on this observation, we then introduce two novel physical-layer metrics: *Interrogation Threshold Power* (ITP): A channel-specific metric that enables accurate link-quality estimation for robust collision resolution, slot assignment, power control, and multi-reader coordination; *Backscatter Power Index* (BPI): A tag-intrinsic, environment-agnostic signature that opens a new avenue for robust battery-free sensing tasks. Finally, we propose an in-situ single-query method that derives these metrics from a single RSSI measurement, cutting measurement overhead by 99.8% over power sweep and reducing channel-estimation error by 64.7%. To-

*Jia Liu is the corresponding author (jialiu@nju.edu.cn).

gether, these contributions deliver high-fidelity signal quality information that the MAC, network, and application layers can directly exploit to enhance throughput, reduce latency, and improve localization and sensing performance in real-world backscatter networks. The main contributions are three-fold.

- We uncover *RSSI compression*, a previously unknown anomaly in RFID backscatter communication, trace it to dynamic RCS behavior, and address it with a refined RCS model and system-level calibration.
- We propose two new physical-layer metrics for robust backscatter network design: ITP for accurate, channel-specific link quality assessment, and BPI for environment- and distance-agnostic measurement, enabling more reliable and scalable backscatter networks.
- Through extensive experiments on commercial off-the-shelf RFID hardware, we show that our proposed metrics can reduce channel estimation errors by 64.7% and improve the measurement efficiency by two orders of magnitude, delivering significant performance gains for backscatter networks.

2 RSSI Distortion

2.1 Traditional RSSI Model

RSSI stands for Received Signal Strength Indicator. It is a measure of the power level of a signal received by a device – in this case, the RFID reader receiving a signal from the tag. In RFID systems, communication relies on electromagnetic waves, and RSSI quantifies the strength of the signal that the reader detects from the tag. Backscatter communication underpins passive RFID systems, enabling tags to transmit data without an internal power source. In this mechanism, a reader emits a continuous radio frequency (RF) wave, which the tag modulates by alternating its antenna impedance between an absorbing state – where it harvests energy – and a backscatter state – where it reflects a portion of the signal to encode information. This reflected signal, detected by the reader using techniques such as amplitude shift keying (ASK), conveys the tag's data through variations in amplitude.

The RSSI measures the power of this backscattered signal at the reader, typically in dBm, serving as a critical metric for assessing link quality. A higher RSSI indicates a stronger signal, improving distinguishability from noise and enhancing communication reliability, yet its accuracy depends on the complex interplay of transmit power, tag behavior, and propagation effects. According to the Friis equation, we have:

$$P_{tag} = P_{tx} \cdot G_{reader} \cdot G_{tag} \cdot (\frac{\lambda}{4\pi R})^2, \tag{1}$$

where P_{tag} is the received power by the tag, P_{tx} is the transmit power by the reader, G_{reader} and G_{tag} are the antenna gains of the reader and the tag antennas, λ is the wavelength of the continuous radio frequency wave, and R is the distance between the reader (antenna) and the tag. Given the two-way backscatter trip (from the reader to the tag and back), we have the power P_{rx} received back at the reader from the tag:

$$P_{rx} = P_{tx} \cdot G_{reader}^2 \cdot G_{tag}^2 \cdot K \cdot (\frac{\lambda}{4\pi R})^4, \tag{2}$$

where K is a backscatter transmission loss. RSSI is the P_{rx} (in Watts) that is converted to milliwatts for the dBm scale:

$$RSSI = P_{rx}^{[dBm]} = 10\log_{10}(P_{rx}/1\text{mW}) = 30 + 10\log_{10} P_{rx}. \tag{3}$$

This equation forms the foundation of RSSI analysis in RFID backscatter communication, widely applied in theoretical studies and system design [12, 13, 21, 33, 39].

2.2 RSSI Compression

In an RFID system, the power received by the reader from the tag's backscatter is proportional to the transmitted power P_{tx}, as expressed in dBm:

$$RSSI = P_{rx}^{[dBm]} = P_{tx}^{[dBm]} + \widetilde{C}^{[dB]}, \tag{4}$$

where $\widetilde{C}$ encapsulates parameters such as antenna gains G_{reader} and G_{tag}, the wavelength λ, the reader-to-tag distance R, and the backscatter transmission loss K. If all system settings (except for P_{tx}) are fixed (i.e., $\widetilde{C}$ is a constant), the RSSI, which measures P_{rx} in dBm, should scale linearly with P_{tx}: A reduction of χ dB in transmit power should thus yield an equivalent χ dB decrease in RSSI:

$$\Delta RSSI = RSSI_1 - RSSI_2 = P_{tx_1}^{[dBm]} - P_{tx_2}^{[dBm]} = \chi. \tag{5}$$

Despite the theoretical elegance of the traditional model, our empirical findings reveal a significant deviation from this expected behavior in practical RFID systems. We conduct experiments in a controlled outdoor environment, designed to approximate free-space conditions. The setup uses a commercial UHF RFID reader (Impinj R420 [4]) and a passive tag (Impinj R6P [5]), with a fixed reader-to-tag distance and environmental conditions. To minimize multipath effects, we place radiation-absorbing materials on the ground to mitigate floor reflections and ensure no strong reflectors are nearby. While not equivalent to an anechoic chamber, this configuration substantially reduces multipath interference, allowing us to focus on the relationship between P_{tx} and RSSI.

In the first experiment, we gradually increase P_{tx} from 14 dBm to 30 dBm in 0.25 dB steps. According to Eq. (5), a 16 dB increase in P_{tx} directly translates to a 16 dB increase in RSSI. However, as shown in Fig. 1, the measured RSSI exhibited a significantly smaller rise, typically less than 8 dB across the 16 dB transmit power range. For instance, when increasing P_{tx} from 20 dBm to 30 dBm, the RSSI rises from -41 dBm to -36.7 dBm – a mere 4.3 dB change – far less

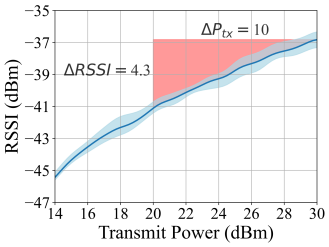

Figure 1: RSSI with respect to the transmit power.

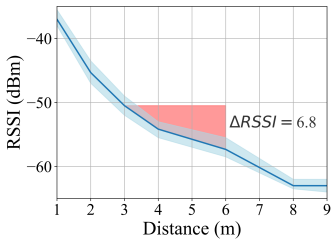

Figure 2: RSSI with respect to the reader-to-tag distance.

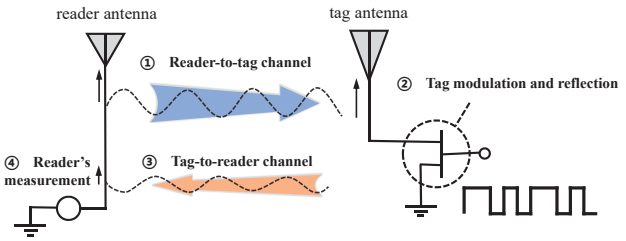

Figure 3: Four components of backscatter communication.

than the expected 10 dB. This discrepancy persists across multiple trials and tag types, indicating a systemic issue rather than an isolated artifact. We note that residual multipath, if present, does not negate this finding. Since multipath effects remain linear increase as P_{tx} varies, the proportionality in Eq. (5) should still hold, yet the observed RSSI behavior consistently deviates from this expectation. This suggests that factors beyond multipath – possibly within the tag's backscatter mechanism or reader receiver characteristics – contribute to the anomaly. We refer to the phenomenon of unexpected RSSI deviation as *RSSI compression*.

To further explore this RSSI compression behavior, we conduct a second experiment examining RSSI variations with reader-to-tag distance R. With P_{tx} fixed at 30 dBm, we increase R from 2 m to 8 m. The traditional model predicts that $P_{rx} \propto \frac{1}{R^4}$ due to the round-trip path loss, meaning a doubling of distance should reduce RSSI by 12 dB ($10\log_{10}(2^4) \approx 12$). However, the measured RSSI again deviates from this expectation. For example, when R increases from 3 m to 6 m, RSSI drops by only 6.8 dB, as shown in Fig. 2. This under-reduction in RSSI further confirms that the traditional model fails to capture the practical dynamics of RFID backscatter communication. If we take the 3 m as the baseline to estimate the reader-to-tag distance, we will misjudge a 6 m ground-truth as near 4 m – a 2 m error caused by RSSI compression.

In summary, these experiments demonstrate that RSSI does not scale linearly with $P_{tx}^{[dBm]}$ or $\frac{1}{R^4}$ (in dB) as predicted by the conventional model. Potential causes for this RSSI compression may include non-linearities in the tag's power harvesting or modulation circuitry, automatic gain control in the reader's receiver, or unaccounted environmental interactions.

3 Causes and RSSI Correction

3.1 Causes of RSSI Compression

The RFID backscatter process begins with the reader transmitting a signal to the tag via the reader-to-tag channel, which determines the power available to activate the tag. Once activated, the tag's behavior – encompassing its modulation and reflection characteristics – generates the backscattered signal. This signal propagates back through the tag-to-reader channel and is finally interpreted by the reader's measurements as RSSI. By examining each part independently, we can pinpoint the source of RSSI anomalies. We decompose the round-trip communication process into four components: (1) The reader-to-tag channel, (2) the tag's behavior (modulation and reflection), (3) the tag-to-reader channel, and (4) the reader's measurements, which are shown in Fig. 3. Through targeted experiments, we isolate each component to determine which is responsible for the observed RSSI anomalies.

3.1.1 Excluding the Reader-to-Tag Channel

We first assess the reader-to-tag channel, which governs the tag's activation. RFID systems are typically downlink-limited, meaning that if a tag receives sufficient power to activate, it can backscatter a readable signal [12]. We test this channel by measuring the minimal transmit power required to activate the tag across varying distances. In an outdoor environment, we vary the reader-to-tag distance from 1 m to 9 m. At each fixed distance, we increase the reader's transmit power P_{tx} in 0.25 dB steps, from its minimum setting until the tag is successfully interrogated for the first time. The minimal transmit power P_{tx}^{min} at which the tag activates and responds to the reader is referred to as the *interrogation threshold power* (ITP). According to the free-space path loss model, the power received by the tag P_{tag} should be proportional to $\frac{1}{R^2}$ (in dB). As distance R doubles, P_{tag} decreases by 6 dB, requiring a 6 dB increase in P_{tx}^{min} to maintain activation. As a consequence, P_{tx}^{min} is supposed to increase 6 dB as the distance R doubles. Fig. 4 shows the results across different distances align with this prediction, which indicates that the reader-to-tag channel is not the source of RSSI anomalies.

3.1.2 Excluding the Tag-to-Reader Channel and Reader

Next, we evaluate the tag-to-reader channel and the reader's measurements by extending the previous experiment to include RSSI measurements at the minimal transmit power. More specifically, at each distance, we determine P_{tx}^{min} with a 0.25 dB resolution and record the RSSI measured by the reader. Since P_{tx}^{min} is adjusted to deliver the same activation power to the tag at each distance, the tag's behavior (modulation and reflection) remains constant. Thus, any RSSI varia-

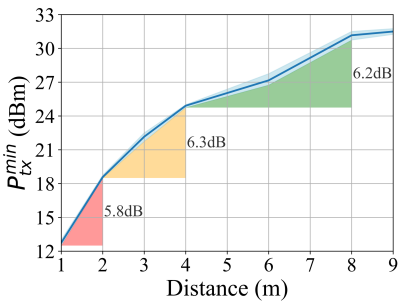

Figure 4: Reader-to-tag channel.

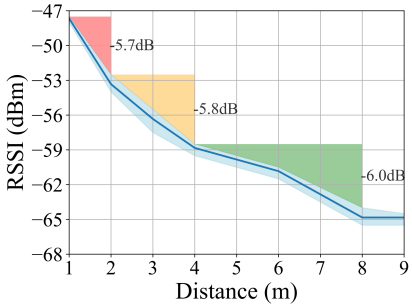

Figure 5: Tag-to-reader RSSI.

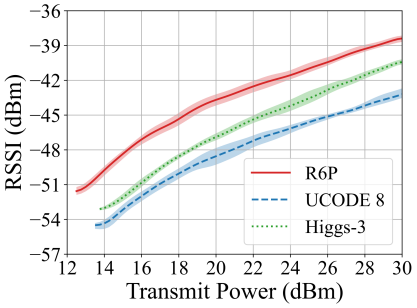

Figure 6: Three tag models' behaviors.

tion would arise from the tag-to-reader channel or the reader.

Theoretically, since the received power P_{tag} by the tag remains stable at the activation power, the tag-to-reader channel introduces a path loss of $\frac{1}{R^2}$, reducing the backscattered signal by 6 dB as distance doubles. As shown in Fig. 5, the RSSI value is proportional to $\frac{1}{R^2}$ (in dB), fluctuating within 0.3 dB as the distance doubles. This result suggests that the tag-to-reader channel and the reader's measurements behave as expected, ruling them out as sources of the RSSI compression.

3.1.3 Identifying the Tag's Behavior as the Cause

With the reader-to-tag channel, tag-to-reader channel, and reader's measurements excluded, we focus on the tag's behavior. To confirm its role, we investigate how different tags respond to varying transmit powers. We test three models of passive UHF RFID tags – Impinj R6P [5], NXP UCODE 8 [6], and Alien Higgs-3 [1] – in a fixed setup (constant distance and environment). For each tag, we measure RSSI across a range of transmit powers P_{tx} in 0.25 dB steps. Existing work assumes that RSSI increases linearly with $P_{tx}^{[dBm]}$ (e.g., a 10 dB rise in P_{tx} should yield a 10 dB increase in RSSI). However, tag-specific factors, such as non-linearities in power harvesting or modulation, could disrupt this relationship.

As shown in Fig. 6, the RSSI responses differ markedly across tags. They have different activation power. Additionally, the RSSI change trends are different either. For example, for a 10 dB increase from 20 dBm to 30 dBm in P_{tx}, the Impinj R6P exhibits a 5.4 dB RSSI increase, the NXP UCODE 8 a 5.5 dB increase, and the Alien Higgs-3 a 6.7 dB increase – none matching the expected 10 dB. This significant variability, despite identical conditions for the channels and reader, confirms that the tag's behavior drives the RSSI anomalies. These discrepancies likely stem from non-linear responses in the tag's circuitry, affecting its backscatter efficiency.

Through systematic experimentation, we demonstrate that the reader-to-tag channel, tag-to-reader channel, and reader's measurements adhere to the traditional path loss model, showing no anomalous behavior. In contrast, the tag's behavior-evidenced by its diverse, non-linear RSSI responses – emerges as the primary cause of RSSI compression in RFID backscatter communication. These findings underscore the need to reconsider RSSI as a reliable metric and account for tag-specific characteristics in RFID system design.

3.2 RSSI in Backscatter Communication

To understand RSSI compression, we must decode how the tag influences RSSI, focusing on its modulation mechanism and the resulting backscatter characteristics. In RFID systems, the RSSI quantifies the power of the backscattered signal received by the reader from a passive tag. Unlike active tags, passive RFID tags rely on backscatter modulation, where they reflect the reader's continuous radio frequency (RF) wave to transmit data. This modulation involves two distinct states: (1) Absorbing state – the tag's antenna impedance is matched to harvest energy from the reader's signal, minimizing reflection and effectively absorbing power. This state typically encodes a binary '0'. (2) Backscatter state – the tag alters its impedance to mismatch the antenna, reflecting a portion of the incident signal back to the reader. This state encodes a binary '1' and is detected via techniques like amplitude shift keying.

The RSSI specifically corresponds to the power received by the reader when the tag is in the backscatter state. This power depends on the tag's radar cross-section (RCS) in the backscatter state (denoted σ), which quantifies its reflective efficiency during backscattering. Traditionally, a higher RCS results in a stronger RSSI, enhancing the signal's distinguishability from noise. Following [14, 16], the RCS of a tag with antenna gain G_{tag} and wavelength λ can be expressed as:

$$\sigma = \left(\frac{\lambda^2}{4\pi}\right) G_{tag}^2 \left|C_l - \Gamma\right|^2, \tag{6}$$

where Γ represents the reflection coefficient and C_l is a constant determined by the length of tag antenna [29, 34, 38]. Γ is determined by the tag impedance, which can be expressed as:

$$\Gamma = \frac{Z_c - Z_a}{Z_c + Z_a}, \tag{7}$$

where Z_c represents the chip impedance, Z_a represents the antenna impedance (a constant determined by the antenna). For sub-half-wavelength antennas (applied by most COTS

tags), we have $C_l \approx 1$, simplifying RCS to:

$$\sigma = \left(\frac{\lambda^2}{4\pi}\right) G_{tag}^2 |1-\Gamma|^2 = \frac{\lambda^2 G_{tag}^2 |Z_a|^2}{\pi |Z_c + Z_a|^2}, \tag{8}$$

which is consistent with prior studies on antennas with near-unity structural scattering constants [25, 29, 38]. Since excessive harvested energy would raise the voltage beyond the IC's tolerance, modern RFID tags dynamically adjust their impedance based on received power levels: Increasing impedance under high RF power to limit energy absorption and decreasing impedance under low RF power to maintain adequate operating voltage. This mechanism renders tag impedance a power-dependent variable, thereby coupling RCS to the incident power. Fig. 7 shows a typical tag architecture given by some commercial tags [8, 31]. As we can see, the chip is connected to functional blocks including clamp, rectification, voltage limiter, and regulation circuitry. These components attenuate voltage to a constant, e.g., 12V, as the input power rises, and vary Z_c consequently. As a result, σ becomes a function of P_{tag}, which can be written as follows:

$$\sigma = f(P_{tag}). \tag{9}$$

In practical use, the function $f(P_{tag})$ is highly non-trivial and influenced by factors such as rectifier topology (e.g., full-bridge vs. half-wave), voltage regulation circuitry, and IC-specific parameters. We can hardly obtain a universal form of $f(P_{tag})$ due to circuit topology variations, e.g., rectifier designs, regulation schemes. To handle this problem, we propose a data driven model that derives $f(P_{tag})$ through real-world experiments. Taking RCS into account, we have the received power P_{rx}:

$$P_{rx} = \frac{P_{tx} \cdot G_{reader}^2 \cdot \lambda^2 \cdot f(P_{tag})}{(4\pi)^3 \cdot R^4}. \tag{10}$$

Expressing P_{rx} in decibel units yields:

$$RSSI = P_{tx}^{[dBm]} + f(P_{tag})^{[dB]} + C^*, \tag{11}$$

where C^* is a constant reflecting hardware and environment parameters such as G_{reader}, wavelength λ, and fixed distance R. On the other hand, according to the experimental results in Fig. 1, *RSSI* approximately experiences a linear grow with the transmit power $P_{tx}^{[dBm]}$:

$$RSSI \approx k \cdot P_{tx}^{[dBm]} + b, \tag{12}$$

where k is the slope and b is the intercept. Comparing Eq. (11) with Eq. (12), we obtain:

$$\sigma^{[dB]} = f(P_{tag})^{[dB]} \approx -\alpha \cdot P_{tx}^{[dBm]} + (b - C^*), \tag{13}$$

where $\alpha = 1 - k$. We can derive k using the least square fitting, which is 0.43 in Fig. 1. The above equation indirectly indicates that RCS can effectively capture the impact of power-dependent tag impedance variations.

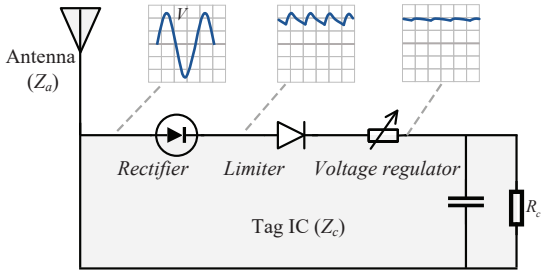

Figure 7: The architecture of RFID tags.

3.3 RSSI Correction

In this subsection, we develop a correction method that decouples the tag's variable RCS effects from the RSSI measurement. The basic idea is to compensate the power differential caused by variable RCS. According to Eq. (10), we reformulate the RSSI expression as:

$$\text{RSSI} = P_{tx}^{[dBm]} - 2\Delta P^{[dB]} + \sigma^{[dB]} + C, \tag{14}$$

where P_{tx} is the transmit power by the reader, ΔP denotes the one-way power loss introduced by the reader-to-tag distance R, σ is the tag's RCS, and C is a hardware-dependent constant. Our correction method enforces a constant RCS for the tag by defining a reference state – where the RCS is artificially fixed. Subsequent RSSI measurements are then corrected by quantifying deviations from this reference. The reference can be pre-measured and is taken as the baseline, denoted as σ_{ref}. During subsequent RSSI measurements, the tag's instantaneous σ deviates from σ_{ref} due to its non-linear backscatter behavior. We derive the corrected RSSI as follows:

$$\begin{aligned} RSSI_{fix} &= P_{tx}^{[dBm]} - 2\Delta P^{[dB]} + \sigma_{ref}^{[dB]} + C \\ &= RSSI + \Delta\sigma^{[dB]}, \end{aligned} \tag{15}$$

where $\Delta\sigma^{[dB]} = \sigma_{ref}^{[dB]} - \sigma^{[dB]}$, which quantifies the deviation between the tag's actual RCS σ and the constant-RCS counterpart σ_{ref}. This correction effectively realigns the measured RSSI with the expected linearized model. Considering $C^* = C - 2\Delta P^{[dB]}$ and Eq. (13), we have:

$$\sigma^{[dB]} \approx -\alpha \cdot P_{tx}^{[dBm]} + b - C + 2\Delta P^{[dB]}. \tag{16}$$

The deviation between two RCSs is:

$$\Delta\sigma = \sigma_{ref}^{[dB]} - \sigma^{[dB]} = \alpha(P_{tx}^{[dBm]} - P_{tx,ref}^{[dBm]}) - 2(\Delta P^{[dB]} - \Delta P_{ref}^{[dB]}), \tag{17}$$

where σ_{ref} represents the reference-state RCS, ΔP is the one-way path loss, $\alpha = 1 - k$ and k is the slope of the linear fitting on $RSSI - P_{tx}$ measurements. The term $\Delta P^{[dB]} - \Delta P_{ref}^{[dB]}$ is equal to the value of $20\log_{10}(\frac{R}{R_{ref}})$, where R_{ref} and R are the reader-to-tag distances in the reference state and in the subsequent measurement phase, respectively. By this means, we obtain $RSSI_{fix}$ that has expected changes as the P_{tx} or the reader-to-tag distance varies.

4 New Metrics: ITP and BPI

RSSI is inherently limited by the tag's dynamic RCS. Although the RSSI correction method compensates the power deviation caused by variable RCS, the value of $\Delta\sigma$ in Eq. (17) is dependent on linear approximation and the reader-to-tag distance, which is often unknown in real-world scenarios. To overcome these shortcomings, we propose the *Interrogation Threshold Power* (ITP), defined as the minimal transmit power P_{tx}^{min} required by the reader to activate the tag, as a superior metric for evaluating the backscatter communication channel. This section explores the advantages of this metric, describes a direct method for obtaining P_{tx}^{min}, and introduces an efficient *Backscatter Power Index* (BPI)-based in-situ measurement technique that leverages only a single query to estimate it.

4.1 ITP vs. RSSI

ITP offers distinct benefits over RSSI for channel evaluation: (1) Channel-specific assessment: Unlike RSSI, which combines the effects of the channel, tag, and reader, ITP isolates the channel's contribution. It represents the minimum power needed to overcome path loss and activate the tag, providing a direct measure of channel quality. It is worth noting that the backscatter communication in RFID is actually a round-trip, including the reader-to-tag channel and the tag-to-reader channel. These two channels are symmetrical – evaluating one of them is sufficient to do the channel assessment. (2) Elimination of tag and reader interference: ITP depends solely on the tag's activation threshold, excluding distortions from the tag's RCS variability or the reader's measurement inconsistencies – both of which compromise RSSI reliability. (3) Enhanced robustness: While RSSI fluctuates with the round-trip channels, ITP focuses on only the downlink from the reader to tag, lowering the impact of channel interference.

4.2 Power Sweep

ITP can be determined through a simple experimental approach: Power sweep. More specifically, we begin with a low transmit power P_{tx} and incrementally increase it until the tag responds to the reader's interrogation. The power level at which the tag first activates is recorded as P_{tx}^{min}. Although this method is straightforward, it requires multiple interrogations, which might suffer from high communication overhead, especially in a tag dense RFID system. For example, Impinj R420 reader has 91 power levels. If we offer each of them a 100 ms interrogation slot, a mean of 4.1 seconds for one measure, which is more than two order of magnitudes compared with the RFID sampling rate – around 21.4 ms per tag with the Impinj R420 reader. Binary searching is an improved method. However, it still needs to do more than 10 power-level search, at least taking one order of magnitude of time over the single sampling. To address this, we propose an in-situ measurement technique that estimates P_{tx}^{min} using just a single traditional RSSI measurement.

4.3 BPI & In-situ Measurement

The in-situ method aims to estimate P_{tx}^{min} using a single RSSI measurement. As aforementioned, the non-linear increase in the tag's radar cross-section σ with received power P_{tag} causes the RSSI to deviate from this expected linear scaling, reducing the RSSI's sensitivity to P_{tx} changes. An intuitive solution involves pre-measuring the RCS $\sigma(P_{tag})$ to derive the dB difference χ between the current transmit power P_{tx} and the expected ITP P_{tx}^{min}. However, this is challenging: $\sigma(P_{tag})$ is determined by the reader-to-tag distance, which is often unknown in practical applications. Specifically, since *RSSI* and the reader's transmit power P_{tx} are known by the user, we reformulate the RSSI expression Eq. (14) as follows:

$$\sigma(P_{tag})^{[dB]} + C - 2\Delta P^{[dB]} = RSSI - P_{tx}^{[dBm]}, \tag{18}$$

where C is a hardware-dependent constant and ΔP is the path loss of the symmetrical channel from the reader to tag and vice versa. When P_{tag} is equal to the tag's activation threshold power P_{tag}^{*}, the transmit power P_{tx} corresponds to ITP P_{tx}^{min} at this time. If the transmit power P_{tx} increases by χ dB, i.e., $P_{tx} = P_{tx}^{min} + \chi$, the power incident on the tag ($P_{tag} = \frac{P_{tx} \cdot G_{reader} \cdot G_{tag} \cdot A_e}{(4\pi R^2)}$) rises, mirroring its χ dB variations exactly and thus altering the RCS (σ) of the tag in its backscatter state. Let $h'(\chi)$ be $\sigma(P_{tag})^{[dBm]} + C - 2\Delta P^{[dB]}$:

$$h'(\chi) = \sigma(P_{tag}^{*[dBm]} + \chi) + C - 2\Delta P^{[dB]} = RSSI - P_{tx}^{[dBm]}. \tag{19}$$

Given a fixed RFID system, we can pre-measure $h'(\chi)$ across various χ values and create a lookup table mapping χ values to $h'(\chi)$, covering the operational range of P_{tx}. In practice, we do a measure of RSSI and calculate $h'(\chi) = RSSI - P_{tx}^{[dBm]}$. With the result of $h'(\chi)$, we figure out χ according to the mapping relationship. The ITP P_{tx}^{min} is equal to $P_{tx} - \chi$. This solution looks good but creates a critical limitation: The path loss ΔP is dependent on the reader-to-tag distance R, which is often unknown in real-world scenarios. This limitation motivates our pursuit of a distance-agnostic method rooted in the invariant backscatter physics of the tag. To eliminate distance dependence, we reformulate the RSSI:

$$\begin{cases} P_{tag}^{[dBm]} = P_{tx}^{[dBm]} - \Delta P^{[dB]} + C' \\ RSSI = P_{tag}^{[dBm]} + \sigma^{[dB]} - \Delta P^{[dB]} + C', \end{cases} \tag{20}$$

where C' is a hardware-dependent constant. We derive a composite metric $h(\chi)$ by combining RSSI and transmit power, which is referred to as *Backscatter Power Index* (BPI):

$$\begin{aligned} h(\chi) &= -RSSI - P_{tx}^{[dBm]} \\ &= -2P_{tag}^{[dBm]} - \sigma(P_{tag})^{[dB]} \\ &= -2(P_{tag}^{*[dBm]} + \chi) - \sigma(P_{tag}^{*[dBm]} + \chi)^{[dB]}. \end{aligned} \tag{21}$$

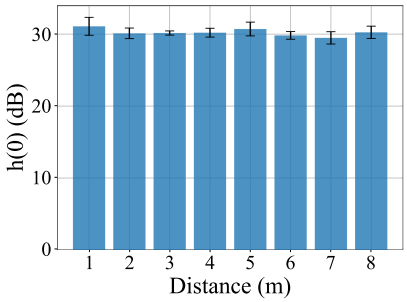

Figure 8: Backscatter power index.

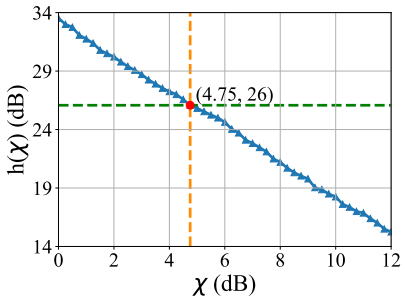

Figure 9: BPI with respect to χ.

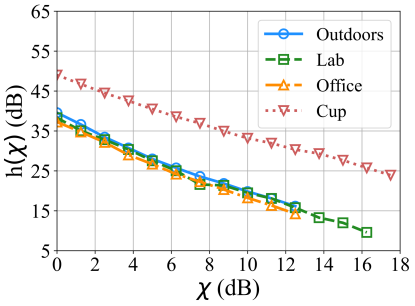

Figure 10: BPI's robustness & potential.

As we can see, the distance-related ΔP is removed from the equation, which means that BPI $h(\chi) = -RSSI - P_{tx}^{[dBm]}$ is a constant when χ is fixed, regardless of the reader-to-tag distance. We validate this conclusion through a real-world experiment. The experimental setup is similar to Fig. 5. In the experiment, we increase the reader-to-tag distance from 1 m to 9 m. At each distance, we adjust the P_{tx} to P_{tx}^{min}, and record the RSSI at the same time. Since P_{tx}^{min} is to deliver the same activation power to the tag at every distance, the power P_{tag} remain unchanged at P_{tag}^{*}. In this case, we have $\chi = 0$ and the BPI $= -RSSI - P_{tx}^{[dBm]}$ is supposed to be a constant $h(0) = -2(P_{tag}^{*[dBm]}) - \sigma(P_{tag}^{*})^{[dB]}$. Fig. 8 plots BPI $h(\chi) = -RSSI - P_{tx}^{[dBm]}$ across different reader-to-tag distances. As we can see, the metric BPI $h(\chi = 0)$ remains stable with very slight fluctuations, regardless of the distance. In contrast, the value of $h'(\chi) = RSSI - P_{tx}^{[dBm]}$ in Eq. (19) varies significantly over different reader-to-tag distances. This positive result well validates the effectiveness and robustness of BPI.

With the above good feature, we can do distance-agnostic and in-situ ITP measurement as follows: First, we build a lookup table mapping the relationship between $h(\chi)$ and χ. Afterward, in practical use, we measure RSSI, calculate $h(\chi) = -RSSI - P_{tx}^{[dBm]}$, and retrieve χ according to the lookup table. We obtain the ITP as follows:

$$P_{tx}^{min[dBm]} = P_{tx}^{[dBm]} - \chi. \tag{22}$$

Fig. 9 illustrates the in-situ measurement through a real-world experiment. The experimental setup is similar to that in Fig. 1, where a commercial UHF RFID reader (Impinj R420 [4]) and a passive tag (Impinj R6P [5]) are deployed, with a fixed reader-to-tag distance (i.e., 2 m) and environmental conditions. We first adjust P_{tx} to figure out P_{tx}^{min}. Afterward, we gradually increase P_{tx} from P_{tx}^{min} to the maximum, in 1 dB steps. A χ dB increase in P_{tx} is equivalent to a mirror of χ dB addition to P_{tag}. Fig. 9 shows the mapping relationship between χ and $h(\chi) = -RSSI - P_{tx}^{[dBm]}$. This is pre-measured only once for later use. In practical use, consider a tag interrogation with $P_{tx} = 30$ dBm and $RSSI = -56$ dBm, where the reader-to-tag distance is unknown and might differ from that when building the lookup table. The composite metric $h(\chi)$ is equal to $-RSSI - P_{tx} = 26$ dB, yielding a $\chi = 4.75$ dB adjustment. Namely, we have $P_{tx}^{min[dBm]} = P_{tx}^{[dBm]} - \chi = 30 - 4.75 = 25.25$ dBm, near the ground truth of 25 dBm.

The in-situ measurement method provides compelling benefits compared to the incremental power adjustment approach: While incremental adjustment requires multiple interrogations – often dozens of power steps to locate P_{tx}^{min} – the in-situ method uses a single and non-intrusive RSSI measurement, drastically reducing measurement time. This efficiency is critical for applications like real-time inventory scanning or mobile RFID systems. This improvement makes the in-situ method a transformative approach for RFID channel evaluation, particularly in fast-paced or resource-constrained applications. The evaluation results show that the in-situ method maintains comparable accuracy to direct measurement, with errors typically around 1 dB, as validated in Section 6.3, ensuring reliability without sacrificing performance. In spite of the advancements, there are two practical considerations. First, $h(\chi)$ profile is unique to each tag model due to differences in circuitry and antenna design. Calibration must account for tags like Impinj R6P or NXP UCODE 8 individually. Second, similar to radar equation that models the free-space power change, the method assumes stable channel conditions during measurement. Significant multipath or interference could distort P_{tag}, so does $h(\chi)$, requiring environmental corrections.

4.4 ITP-based Channel Estimation

With estimated ITP, we can easily derive the reader-to-tag distance R by quantifying deviations from a reference as baseline. More specifically, according to Eq. (20), we have:

$$P_{tag}^{*[dBm]} = P_{tx}^{min[dBm]} - \Delta P^{[dB]} + C', \tag{23}$$

where C' is a hardware-dependent constant and $\Delta P^{[dB]} = 20\log_{10} R$ denotes the one-way power loss introduced by the reader-to-tag distance R. The difference between $P_{tx}^{min[dBm]}$ and $P_{tx,ref}^{min[dBm]}$ mirrors the dB variation exactly caused by $\Delta P^{[dB]} - \Delta P_{ref}^{[dB]} = 20\log_{10}(\frac{R}{R_{ref}})$. Thus, we have:

$$R = R_{ref} \cdot 10^{(P_{tx}^{min[dBm]} - P_{tx,ref}^{min[dBm]})/20}. \tag{24}$$

The ranging accuracy of ITP will be given in Section 6.3.

5 Discussion

5.1 BPI: A Robust Tag-intrinsic Power Metric

Although initially developed as an intermediate step for deriving single-sample ITP, our proposed Backscatter Power Index (BPI) exhibits significant potential for IoT sensing applications due to its environment- and distance-agnostic properties. As derived in Eq. (21), the BPI, denoted $h(\chi)$, depends solely on the tag's received power P_{tag} and is independent of path loss ΔP or environmental factors like multipath. This invariance stems from the cancellation of ΔP during the subtraction of RSSI and P_{tx}, rendering $h(\chi)$ a tag-intrinsic property for a given excess power $\chi = P_{tx} - P_{tx}^{min}$. This robustness makes BPI well-suited for reliable sensing applications, such as material detection in a black-box scenario or tag-based touch interactions for human-computer interfaces, where variations in $h(\chi)$ reflect tag-material interactions (e.g., dielectric changes) rather than distance or environmental effects.

Fig. 10 illustrates the behavior of BPI $h(\chi)$ versus χ for an Impinj R6P tag across four scenarios:a tagged plastic ruler in an outdoor setting (near free-space conditions), an office room (moderate multipath), a laboratory (heavy multipath with many metallic reflections), and a tagged ceramic cup, as depicted in Fig. 11. The results show a consistent trend in $h(\chi)$ across the outdoor, office, and laboratory scenarios, driven solely by χ, demonstrating BPI's environment-agnostic nature. Even in the heavily multipath laboratory setting, BPI remains stable, underscoring its tag-intrinsic property. For the tagged cup, BPI exhibits a significant shift due to impedance changes induced by the ceramic material, which alters the tag's RCS, enabling material property detection. These characteristics make BPI ideal for applications such as black-box material characterization, where tag-intrinsic changes must be detected reliably despite environmental variability.

5.2 Benefits Across the RFID Network Stack

MAC-layer Enhancements. At the MAC layer, ITP and BIP enable precise channel assessment, improving collision resolution and dynamic slot assignment in dense tag environments, thus reducing read latency and boosting throughput. For example, parallel decoding techniques, like those in [17, 27], rely on accurate in-phase and quadrature (IQ) signal components, which are derived from RSSI, to decode multiple tags simultaneously. One signal sample from multiple tags received at physical layer is represented as one complex symbol on the IQ plane. Multiple received symbols from the same collision state are dispersed and scattered around a centroid position, forming a cluster. The key to parallel decoding is to identify the number of clusters and the symbols belonging to each cluster. RSSI compression shortens the inter-cluster distance, reducing decoding accuracy. Similarly, dynamic slot assignment, as explored in [20], adaptively adjusts MAC-layer slot counts based on tag motion. Specifically, RSSI serves as a critical indicator for detecting tag mobility. Mobile tags suffer from more variations on RSSI, thereby requiring more time slots to be read. However, when RSSI is compressed, its transient fluctuation patterns might be smoothed out, leading to misclassification of mobile tags.

Network and Transport Layer Improvements. At the network and transport layers, RSSI compression can overestimate link quality, leading to failed handovers between readers, or underestimate it, causing redundant retransmissions that degrade network efficiency [10, 28]. On one hand, overestimation occurs when the tag's RCS increases at small received power, making the measured RSSI appear stronger than the actual link quality, which can cause the system to maintain a weakening connection longer than necessary. On the other hand, underestimation arises when RCS decreases at high power, causing RSSI to drop less than anticipated and portraying the link as weaker, prompting unnecessary caution in data handling. Consider a handover scenario [28] with two readers, A and B, where a tag moves from A's coverage to B's: As the tag recedes from A, the actual RSSI drops, but compression results in a measured RSSI that remains artificially high (overestimation), delaying A's release of the tag; concurrently, as the tag approaches B, the actual RSSI rises, but compression yields a measured RSSI that increases slowly (underestimation), delaying B's activation. This mismatch leads to coverage gaps during the transition, resulting in a brief "blackout" and even missed reads. Additionally, underestimation makes the reader retransmit queries to verify potentially corrupted data [10], even if the initial read succeeded, increasing network contention and latency in multi-tag environments. In contrast, our physical-layer metrics address RSSI compression, which enhances link-quality estimation and routing decisions, enabling reliable communication and robust handovers in multi-reader deployments.

Application-layer Advancements. At the application layer, accurate RSSI enables selective querying in dense IoT deployments like smart logistics, minimizing cross-reading and enhancing system reliability [19]. Beyond communication performance, many emerging IoT sensing applications increasingly rely on RSSI as a key signal feature. For example, RSSI-based localization and trajectory tracking [41, 42, 44] in warehouses or retail environments critically depend on accurate signal strength readings to estimate tag positions with minimal error. Similarly, RFID-based environmental sensing applications, where tags act as battery-free sensors measuring soil moisture [35], material [36], or human behavior [22], often correlate changes in backscatter strength with physical parameters; thus, ITP's improved RSSI measurement accuracy directly translates into more precise and reliable sensing results. Furthermore, our proposed BPI is environment- and distance-agnostic, which opens up a new avenue in robust

Figure 11: Experimental setup.

sensing applications such as material characterization and human-computer interaction. In summary, our physical-layer observations strengthen cross-layer optimization by delivering a clean, high-fidelity signal-quality metric that higher layers can reliably use to improve overall system performance.

5.3 Impact of Other Factors

Reader's Automatic Gain Control. The RFID reader's signal processing can influence RSSI measurements, notably through Automatic Gain Control (AGC). AGC dynamically adjusts the receiver's gain to maintain a stable output signal strength, compensating for variations in input power caused by changes in P_{tx} or distance. In some readers, aggressive AGC may compress RSSI values, especially at high P_{tx}, as the receiver scales down the signal to prevent saturation. This could exacerbate RSSI compression. Notably, the readers (i.e., Impinj and Alien readers) used in our experiments have minimal AGC impact, ensuring RCS dominance, likely due to two reasons: First, these readers are designed with sophisticated receiver architectures that minimize AGC's impact on RSSI measurements. Second, AGC may compress RSSI if the input signal approaches the receiver's saturation threshold or if low-power signals trigger excessive gain boosts. However, our measured RSSI values typically range from -60 to -40 dBm, well within the linear range of tested readers. Future work could explore readers with more aggressive AGC to quantify their secondary contributions, but our findings hold for high-performance readers like those used.

Auto-tune Functionality in Advanced Tags. Advanced RFID tags, such as those with NXP UCODE 8 chips, incorporate auto-tune functionality to optimize power harvesting by adjusting antenna impedance. This feature is particularly effective for adapting to different materials (e.g., metals, woods), enhancing sensitivity in diverse applications. However, in our experiments conducted in air with NXP UCODE 8 tags, the auto-tune function remained stable, as the consistent dielectric properties of air required minimal impedance adjustments. When tags are placed near materials with varying permittivity (e.g., cardboard, water), auto-tune dynamically modifies RCS, potentially exacerbating RSSI compression. To address this, we recommend pre-checking the material environment to calibrate RCS models or using tags without auto-tune (e.g., Impinj R6P) or disabling auto-tune where supported.

Multipath Effects. Multipath effects, where signals reflect off surfaces and interfere at the receiver, can impact both RSSI and ITP. Consistent with the Friis equation, our study primarily models power transfer under free-space or weak multipath conditions, where the derived metrics remain meaningful for network stack optimization and IoT applications as mentioned above. Compared with conventional RSSI, ITP mitigates the influence of the tag's RCS, providing a more precise channel measurement. While our current focus is on alleviating RSSI compression and enhancing signal fidelity, integrating explicit multipath models, e.g., through differential measurement or phase-based analysis, represents a promising direction for future work beyond the current study's scope.

6 Evaluation

The experimental setup is illustrated in Fig. 11. To ensure generalizability, we evaluate our methodology using RFID devices from three leading manufacturers: Impinj, Alien, and NXP. The reader models include Impinj R420 [4], Alien ALR-9900+ [2], and Alien ALR-F800 [3], all mounted on a TE PAV90209H-FNF antenna [7], supporting RSSI measurements during tag inventory operations. Three tag models are tested: Impinj R6P (ER62) [5], Alien Higgs-3 (9640) [1], and NXP UCODE 8 (9662) [6]. A host laptop (Intel Core i5-220H, 2.7 GHz, 16 GB RAM) controls the readers via Java-based software implementing the EPC Gen2 low-level reader protocol (LLRP) for standardized communication. To approximate free-space conditions, experiments are conducted outdoors, with radiation-absorbent materials minimizing ground reflections. The other three scenarios are used for BPI.

6.1 RSSI Compression

We first validate whether different tag models all have the problem of RSSI compression. Three tag models including Impinj R6P [5], NXP UCODE 8 [6], and Alien Higgs-3 [1] are tested. For each tag model, three readers Impinj R420 [4], Alien ALR-9900+ [2], and Alien ALR-F800 [3] are adopted. In the first experiment, we validate the RSSI compression with regard to the transmit power. In the experiments, we

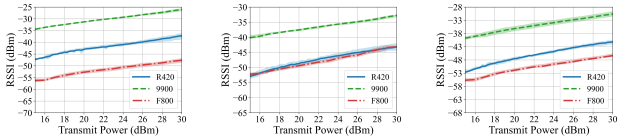

(a) R6P (b) UCODE 8 (c) Higgs-3

Figure 12: RSSI with respect to the transmit power.

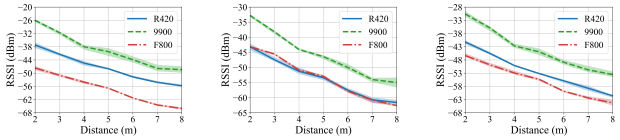

(a) R6P (b) UCODE 8 (c) Higgs-3

Figure 13: RSSI with respect to the reader-to-tag distance.

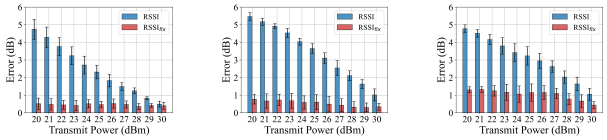

(a) R6P (b) UCODE 8 (c) Higgs-3

Figure 14: Correction error with respect to the transmit power.

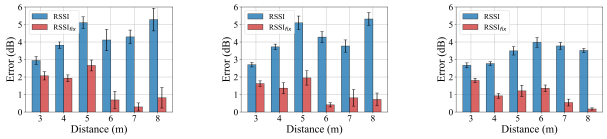

(a) R6P (b) UCODE 8 (c) Higgs-3

Figure 15: Correction error with respect to the distance.

gradually increase the transmit power P_{tx} from 15 dBm to 30 dBm in 0.25 dB (Impinj readers) or 1 dB steps (Alien readers). As shown in Fig. 12, all tag-reader combinations exhibit significant deviations from the theoretical one-to-one slope – RSSI compression all exist across the three tag models. For example, Fig. 12 shows that, with the Impinj R420 reader, the Impinj R6P exhibits a 5.2 dB RSSI increase, the NXP UCODE 8 has a 5.0 dB increase, and the Alien Higgs-3 experiences a 6.3 dB rise, all far less than the expected 10 dB when P_{tx} increase from 20 dBm to 30 dBm. This discrepancy persists across multiple trials and tag types. Additionally, we also observe that the RSSI plots under the three different reader models have similar change trend, which indicates that the readers have small impact on the RSSI-compression issue.

To further explore the RSSI compression behavior, we examine RSSI variations with the respect to the reader-to-tag distance. In the experiment, we fix the transmit power to 30 dBm, and increase the distance from 2 m to 8 m. Since $P_{rx} \propto \frac{1}{R^4}$ due to the round-trip path loss, meaning a doubling of distance (e.g., from 2 m to 4 m) should reduce RSSI by 12 dB. However, as shown in Fig. 13, the measured RSSI again deviates from this expectation. For example, given the Impinj R420 reader with the distance increasing from 2 m to 4 m, the Impinj R6P exhibits a 7.8 dB RSSI reduction, the NXP UCODE 8 experiences a 8.5 dB decline, and the Alien Higgs-3 has a 8.9 dB change, all far less than the expected 12 dB. This consistent under-reduction in RSSI further confirms that the traditional model fails to capture the practical dynamics of RFID backscatter communication. Notably, since the two readers behavior similarly, we use Impinj R420 as default to evaluate the performance in what follows.

6.2 RSSI Correction

We next study the performance of RSSI correction proposed in Section 3.3. Similar to the experiments in RSSI compression, we validate the deviation from the expected RSSI. In Fig. 14, we fix the reader-to-tag distance to 2 m and first obtain a reference RSSI at the transmit power of 32.5 dBm. After that, we gradually decrease the transmit power from 30 dBm to 20 dBm in 1 dB steps. As shown in this figure, due to RSSI compression, the error of raw RSSI becomes larger as the transmit power is far away from 32.5 dBm. However, our RSSI correction method makes the fixed RSSI close to the expected RSSI. For example, the maximized deviations of R6P, UCODE 8, and Higgs-3 are 0.5 dB, 0.8 dB, and 1.3 dB across all the transmit power range, respectively. These small errors validate the effectiveness of our RSSI correction method. The performance difference among different tags might be due to the linear-assumption fits differently on the three kinds of tags. We further validate the RSSI correction over difference reader-to-tag distances. In the experiment, we first fix the distance to 2 m and to calibrate RSSI using the RSSI profile under different transmit powers. After that, we test all transmit powers and validate the correction accuracy over different distances. Fig. 15 shows that our fixed RSSI has much smaller errors compared with the raw RSSI, which further validates the effectiveness of our proposed method.

6.3 Performance of BPI & ITP

Robustness of BPI. We validate whether BPI is tag-intrinsic and distance-agnostic. In the experiment, we dynamically change $\chi = P_{tag} - P^*_{tag}$ for checking the tag's characteristic and the reader-to-tag distance for studying the robustness to the distance. As shown in Fig. 16, we can see that BPI is dependent on P_{tag}: it varies largely as χ changes (equivalent to P_{tag} changes). For example, given the R6P tag with fixed 2 m distance, a 18 dB increase of χ gives rise to about 30 dB decrease of BPI. However, once χ is fixed, BPI almost remain stable, regardless of the reader-to-tag distances. This conclusion can be drawn across all three tag models, which well indicate that our proposed BPI is tag-intrinsic and distance-

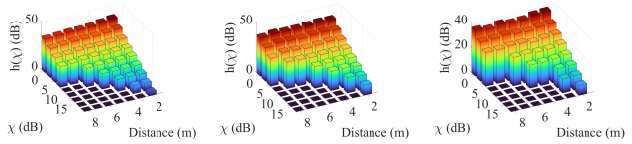

(a) R6P (b) UCODE 8 (c) Higgs-3

Figure 16: Robustness of BPI: $h(\chi)$.

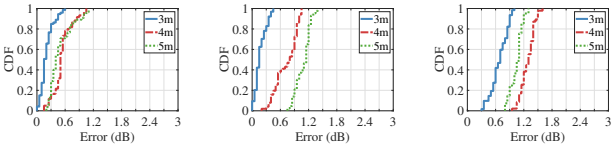

(a) R6P (b) UCODE 8 (c) Higgs-3

Figure 17: Error of the in-situ method.

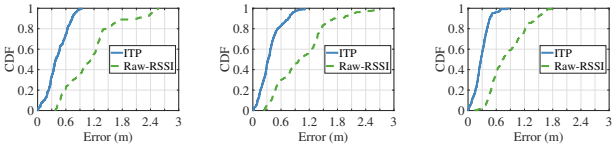

(a) R6P (b) UCODE 8 (c) Higgs-3

Figure 18: Error of ITP-based distance estimation.

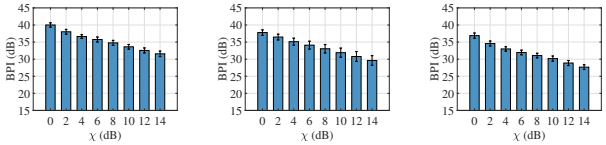

(a) R6P (b) UCODE 8 (c) Higgs-3

Figure 19: Tag diversity on BPI.

agnostic. This provides us with a robust foundation for our in-situ ITP measurement in practical RFID systems.

Accuracy of In-situ Measurement. In this study, we validate the accuracy of our proposed in-situ measurement method. The ground truth is obtained by the power sweep from the minimal power to the one the first time to activate the tag. The in-situ measurement takes BPI with 2 m reader-to-tag distance as the reference (which is pre-measured). Fig. 17 shows the CDF of the estimate errors by our in-situ measurement over different reader-to-tag distances. It is clear that the measurement error of the three tag models is small. For example, the 80th percentile of R6P is within 0.7 dB, UCODE 8 is within 1.2 dB, and Higgs-3 is less than 1.4 dB, over different distances. This is due to the good robustness of BPI. In spite of some small accuracy loss, the time efficiency of measurement is significantly improved.

Time Efficiency of In-situ Measurement. We next study the time efficiency of our in-situ measurement, taking the power sweep method as the baseline for comparison. For power sweep, each power-level needs an interrogation slot for querying potential tags. Since we do not have the knowledge of the tag cardinality at each power level in advance, the setting of the slot length is a dilemma: Long slots waste the running time (some power levels do not have any tags) while short slots might miss some tags (i.e., a power-level corresponds to many tags, leading to slot competition). In this experiment, we experientially set the interrogation slot to 100 ms for a trade-off. As shown in Table 1, we test the measurement time over different ITP, from 10 to 28 dBm. The power sweep begins from the minimal power 10 dBm and the running time increases linearly as the ITP increases because more power search is needed. In contrast, our in-situ measurement takes a constant time: Around 21 ms – the sampling rate of a single tag by Impinj R420. As we can see, we can improve the time efficiency significantly. For example, when ITP is at the minimum 10 dBm, the power sweep method achieves optimal performance by requiring only a single power level check. In this case, the total identification time for R6P is 268.9 ms, which includes a 100 ms slot duration and approximately 170 ms of switching overhead between adjacent power levels. For the average case where ITP is 19 dBm, our in-situ method reduces the time overhead by 99.8%,

Channel Estimation. We compare the distance estimation accuracy of RSSI and ITP methods by analyzing the CDF of estimation errors (in meters) across the three tag models: Impinj R6P [5], NXP UCODE 8 [6], and Alien Higgs-3 [1]. As shown in Fig. 18, ITP consistently outperforms RSSI, achieving sub-meter median error across all tags, while RSSI exhibits much higher variance. For example, the 80th percentile of ITP's errors are 0.63 m, 0.51 m, 0.40 m, for R6P, UCODE 8, Higgs-3, respectively. In contrast, the 80th percentile of RSSI's errors are 1.38 m, 1.47 m, 1.21 m, for R6P, UCODE 8, Higgs-3, respectively. It reduces errors by 64.7% on average. These positive results validate the potential of in-situ ITP measurement for high-accuracy passive IoT network.

Tag Diversity. To evaluate the impact of tag diversity on BPI, we test 30 tags – 10 from each of three models (Impinj R6P, NXP UCODE 8, and Alien Higgs-3). We conduct single-query measurements on multiple tags at the same time, with EPC Gen2 ensuring anti-collision communication. As shown in Fig. 19, BPI exhibits high intra-model consistency, with average deviations under 1 dB for tags of the same model. This uniformity enables model-level calibration – eliminating per-tag registration and thus reducing deployment effort. Inter-model comparisons, however, reveal relatively distinct BPI signatures (e.g., 2∼4 dB differences between Impinj and NXP tags), attributed to variations in antenna geometry and chip impedance. These results validate BPI's dual utility: A tag-agnostic metric within models for scalable deployments, and

Table 1: Measurement Time Comparison (ms)

Tag Model	Method	ITP (dBm)						
		10	13	16	19	22	25	28
R6P	Power Sweep	268.9	3507.6	6714.0	10076.0	13036.4	16458.6	19421.5
	In-situ Measurement	**21.4**	**21.5**	**21.4**	**21.7**	**21.2**	**21.5**	**21.2**
UCODE 8	Power Sweep	269.5	3513.1	6756.0	9998.9	13241.8	16329.2	19727.6
	In-situ Measurement	**21.2**	**21.2**	**21.2**	**21.2**	**21.2**	**21.0**	**21.2**
Higgs-3	Power Sweep	271.7	3567.7	6796.2	10058.3	13257.0	16582.6	19844.8
	In-situ Measurement	**21.0**	**21.2**	**21.0**	**21.0**	**20.9**	**21.0**	**21.0**

a model-discriminative feature for heterogeneous networks, ensuring reliable performance without per-device overhead.

7 Related Work

Received Signal Strength Indicator (RSSI) has been long a cornerstone metric in backscatter communication. It quantifies the strength of the signal modulated by the tag in its backscatter state, typically measured in dBm. As a standard output of RFID readers, RSSI serves as a fundamental metric for assessing link quality, widely guiding localization [24,41,42,44] and sensing [23, 36, 40, 43, 45] research and applications. In localization, RSSI enables distance estimation and tag positioning, critical for applications like warehouse inventory tracking and retail asset management. For example, LANDMARC [24] introduces the concept of RFID fingerprinting, which locates tag position by comparing RSSI similarity between neighboring reference tags. Recent AI-based approaches leverage RSSI to train a neural network to model RF radiation field for localization [44]. In sensing, GreenTag [35] employs dual RFID tags and an RSSI-based metric called DMRT to enable soil moisture monitoring in greenhouses. RF-EATS [15] identifies food and liquids by analyzing RSSI and phase changes of RFID tags in complex multi-path scenarios. Tag-Compass [21] proposes high-precision direction detection based on single tag by analyzing RSSI changes caused by polarization.

Despite its widespread adoption, RSSI's non-linear scaling with the transmit power and the reader-to-tag distance limits its reliability, motivating our investigation into tag-induced anomalies. Traditional RSSI modeling in RFID systems typically employs the Friis equation, which expresses the received power as proportional to the reader's transmit power [12, 13, 18, 21, 33, 39]. However, these models often fail to account for RSSI deviations when the transmit power varies, a phenomenon has been commonly ignored but was observed by our practical setups. Some prior wireless research has recognized RCS as a factor influencing the received power [14, 16, 25, 32, 34, 38], primarily focusing on accurately modeling RCS or measuring it in real-world systems. However, these studies do not address the system-level implications of RCS variations on RSSI measurements. Instead, our work introduces a novel contribution by identifying and characterizing the unknown phenomenon of RSSI compression in passive RFID networks. Beyond merely analyzing RCS, we design experiments to pinpoint the root cause of RSSI compression, design a calibration framework to correct for compression effects, and propose two new metrics that enable accurate link quality assessment and environment-agnostic sensing. Together, these contributions move beyond traditional RCS studies toward solving a critical, unexplored measurement challenge in backscatter systems.

8 Conclusion

This work uncovers RSSI compression, a previously unknown anomaly in RFID backscatter networks, and traces it to the power-dependent nonlinear RCS behavior of passive tags. We show that this physical-layer distortion propagates across the network stack, degrading MAC-layer collision resolution, network-layer link estimation, and application-layer system reliability. To address this challenge, we introduce two physical-layer metrics: ITP for accurate link-quality assessment and BPI for environment-agnostic measurement. Together with our in-situ single-query measurement, these metrics reduce channel-estimation error by 64.7% and measurement overhead by 99.8%. We believe this work provides a foundation for reliable, high-performance backscatter and IoT networks.

Acknowledgments

We would like to thank our shepherd, Prof. Venkat Arun, and the anonymous reviewers for their insightful comments. This work was supported in part by the National Natural Science Foundation of China (Nos. 62332013, 62032017, 62272368, 62172276, 62372296, 62441236), the Jiangsu Natural Science Foundation (No. BK20241247), the China Postdoctoral Science Foundation (No. GZB20240306), the Jiangsu Funding Program for Excellent Postdoctoral Talent (No. 2024ZB504), the Fundamental Research Funds for the Central Universities (No. 14380134), the Collaborative Innovation Center of Novel Software Technology and Industrialization, the Shaanxi Innovation Capability Support Program (No. 2023-CX-TD-08), the Key Talent Project of Xidian University (No. QTZX24004), and the Shaanxi Qinchuangyuan "Scientists+Engineers" Team (No. 2023KXJ-040).

References

[1] Alien 9640. https://www.alientechnology.com/products/tags/squiggle/.

[2] ALR 9900+. https://www.alientechnology.com/products/files-2/alr-9900/.

[3] ALR F800. https://www.alientechnology.com/products/readers/alr-f800/.

[4] Impinj R420. https://www.impinj.com/products/readers/impinj-speedway.

[5] Impinj R6P. https://www.impinj.com/products/tag-chips/impinj-monza-r6-series.

[6] NXP UCODE 8. https://www.nxp.com/products/rfid-nfc/ucode-rain-rfid-uhf:MC_50483.

[7] PAV90209H-FNF. https://www.te.com.cn/chn-zh/product-PAV90209H-FNF.html.

[8] Ganesh K Balachandran and Raymond E Barnett. Voltage regulation circuit for RFID systems, 2009. US Patent 7,538,673.

[9] Xingyu Chen, Jia Liu, Xia Wang, Haisong Liu, Dong Jiang, and Lijun Chen. Eingerprint: Robust energy-related fingerprinting for passive RFID tags. In *Proc. of USENIX NSDI*, pages 1101–1113, 2020.

[10] Yen-Hung Chen, Rui-Ze Hung, Lin-Kung Chen, Pi-Tzong Jan, and Yin-Rung Su. Channel-quality aware RFID tag identification algorithm to accommodate the varying channel quality of Io environment. *Applied Sciences*, 9(2), 2019.

[11] Donghui Dai, Zhenlin An, Zheng Gong, Qingrui Pan, and Lei Yang. RFID+: Spatially controllable identification of UHF RFIDs via controlled magnetic fields. In *Proc. of USENIX NSDI*, pages 1351–1367, 2024.

[12] Daniel Dobkin. *The RF in RFID: UHF RFID in practice*. Newnes, 2012.

[13] Alessandro Felaco, Kamil Yavuz Kapusuz, Hendrik Rogier, and Dries Vande Ginste. Efficient modeling of on-body passive UHF RFID systems in the radiative near-field. *IEEE Transactions on Antennas and Propagation*, 70(4):2979–2989, 2021.

[14] Robert Blair Green. *The general theory of antenna scattering*. The Ohio State University, 1963.

[15] Unsoo Ha, Junshan Leng, Alaa Khaddaj, and Fadel Adib. Food and liquid sensing in practical environments using RFIDs. In *Proc. of USENIX NSDI*, pages 1083–1100, 2020.

[16] Roger F. Harrington. Electromagnetic scattering by antennas. *IEEE Transactions on Antennas and Propagation*, 11(5):595–596, 1963.

[17] Meng Jin, Yuan He, Xin Meng, Dingyi Fang, and Xiaojiang Chen. Parallel backscatter in the wild: When burstiness and randomness play with you. In *Proc. of ACM MobiCom*, page 471–485, 2018.

[18] Chenglong Li, Emmeric Tanghe, David Plets, Pieter Suanet, Jeroen Hoebeke, Eli De Poorter, and Wout Joseph. Reloc: Hybrid RSSI- and phase-based relative UHF-RFID tag localization with COTS devices. *IEEE Transactions on Instrumentation and Measurement*, 69(10):8613–8627, 2020.

[19] Bo Liang, Purui Wang, Renjie Zhao, Heyu Guo, Pengyu Zhang, Junchen Guo, Shunmin Zhu, Hongqiang Harry Liu, Xinyu Zhang, and Chenren Xu. RF-Chord: Towards deployable RFID localization system for logistic networks. In *Proc. of USENIX NSDI*, pages 1783–1799, 2023.

[20] Qiongzheng Lin, Lei Yang, Huanyu Jia, Chunhui Duan, and Yunhao Liu. Revisiting reading rate with mobility: Rate-adaptive reading in COTS RFID systems. In *Proc. of ACM CoNEXT*, page 199–211, 2017.

[21] Jia Liu, Min Chen, Shigang Chen, Qingfeng Pan, and Lijun Chen. Tag-compass: Determining the spatial direction of an object with small dimensions. In *Proc. of IEEE INFOCOM*, pages 1–9, 2017.

[22] Jia Liu, Xingyu Chen, Shigang Chen, Xiulong Liu, Yanyan Wang, and Lijun Chen. TagSheet: Sleeping posture recognition with an unobtrusive passive tag matrix. In *Proc. of IEEE INFOCOM*, pages 874–882, 2019.

[23] Massimo Merenda, Giuseppe Cimino, Riccardo Carotenuto, Francesco G Della Corte, and Demetrio Iero. Edge machine learning techniques applied to RFID for device-free hand gesture recognition. *IEEE Journal of Radio Frequency Identification*, 6:564–572, 2022.

[24] Lionel M Ni, Yunhao Liu, Yiu Cho Lau, and Abhishek P Patil. LANDMARC: Indoor location sensing using active RFID. In *Proc. of IEEE PerCom 2003.*, pages 407–415. IEEE, 2003.

[25] Pavel V Nikitin and KVS Rao. Measurement of backscattering from RFID tags. In *Proc. of Antennas Measurement Techniques Association Symposium*, pages 425–443. Citeseer, 2005.

[26] Mugahid Omer and Gui Yun Tian. Indoor distance estimation for passive UHF RFID tag based on RSSI and RCS. *Measurement*, 127:425–430, 2018.

[27] Jiajue Ou, Mo Li, and Yuanqing Zheng. Come and be served: Parallel decoding for COTS RFID tags. In *Proc. of ACM MobiCom*, pages 500–511, 2015.

[28] Apostolia Papapostolou and Hakima Chaouchi. Handoff management relying on RFID technology. In *Proc. of IEEE WCNC*, pages 1–6, 2010.

[29] Robert K. Schneider. A re-look at antenna in-band RCSR via load mismatching. In *IEEE Antennas and Propagation Society International Symposium. 1996 Digest*, volume 2, pages 1398–1401 vol.2, 1996.

[30] Longfei Shangguan, Zheng Yang, Alex X Liu, Zimu Zhou, and Yunhao Liu. Relative localization of RFID tags using spatial-temporal phase profiling. In *Proc. of USENIX NSDI*, pages 251–263, 2015.

[31] Pairote Sirinamaratana and Pattrakorn Chokchalermwat. Voltage regulator circuit for RFID circuit, 2025. US Patent 12,216,486.

[32] S. Skali, C. Chantepy, and S. Tedjini. On the measurement of the delta radar cross section (RCS) for UHF tags. In *Proc. of IEEE RFID*, pages 346–351, 2009.

[33] Saurav Subedi, Eric Pauls, and Yimin D Zhang. Accurate localization and tracking of a passive RFID reader based on RSSI measurements. *IEEE Journal of Radio Frequency Identification*, 1(2):144–154, 2017.

[34] Johnson J. H. Wang, Chang W. Choi, and RICK L. Moore. Precision experimental characterization of the scattering and radiation properties of antennas. *IEEE Transactions on Antennas and Propagation*, 30(1):108–112, 1982.

[35] Ju Wang, Liqiong Chang, Shourya Aggarwal, Omid Abari, and Srinivasan Keshav. Soil moisture sensing with commodity RFID systems. In *Proc. of ACM MobiSys*, pages 273–285, 2020.

[36] Ju Wang, Jie Xiong, Xiaojiang Chen, Hongbo Jiang, Rajesh Krishna Balan, and Dingyi Fang. TagScan: Simultaneous target imaging and material identification with commodity RFID devices. In *Proc. of ACM MobiCom*, pages 288–300, 2017.

[37] Jue Wang and Dina Katabi. Dude, where's my card? RFID positioning that works with multipath and non-line of sight. In *Proc. of ACM SIGCOMM*, pages 51–62, 2013.

[38] Werner Wiesbeck and Eberhardt Heidrich. Wide-band multiport antenna characterization by polarimetric RCS measurements. *IEEE Transactions on Antennas and Propagation*, 46(3):341–350, 1998.

[39] Binbin Xie, Jie Xiong, Xiaojiang Chen, Eugene Chai, Liyao Li, Zhanyong Tang, and Dingyi Fang. Tagtag: Material sensing with commodity RFID. In *Proc. of ACM SenSys*, pages 338–350, 2019.

[40] Weiye Xu, Jianwei Liu, Shimin Zhang, Yuanqing Zheng, Feng Lin, Jinsong Han, Fu Xiao, and Kui Ren. Rface: Anti-spoofing facial authentication using COTS RFID. In *Proc. of IEEE INFOCOM*, pages 1–10, 2021.

[41] Lei Yang, Qiongzheng Lin, Xiangyang Li, Tianci Liu, and Yunhao Liu. See through walls with COTS RFID system! In *Proc. of ACM MobiCom*, pages 487–499, 2015.

[42] Lei Yang, Yong Qi, Jianbing Fang, Xuan Ding, Tianci Liu, and Mo Li. Frogeye: Perception of the slightest tag motion. In *Proc. of IEEE INFOCOM*, pages 2670–2678. IEEE, 2014.

[43] Yinggang Yu, Dong Wang, Run Zhao, and Qian Zhang. RFID based real-time recognition of ongoing gesture with adversarial learning. In *Proc. of ACM SenSys*, pages 298–310, 2019.

[44] Xiaopeng Zhao, Zhenlin An, Qingrui Pan, and Lei Yang. Nerf2: Neural radio-frequency radiance fields. In *Proc. of ACM MobiCom*, pages 1–15, 2023.

[45] Yinan Zhu and Qian Zhang. LoPrint: Mobile authentication of RFID-tagged items using COTS orthogonal antennas. In *Proc. of IEEE INFOCOM*, pages 1551–1560, 2024.